Petroleum Science 20 (2023) 3530–3539

Contents lists available at ScienceDirect

Petroleum Science

journal homepage: www.keaipublishing.com/en/journals/petroleum-science

Original Paper

Molecular design and applications of a nanostructure green Tripodal surface active ionic liquid in enhanced oil recovery: Interfacial tension reduction, wettability alteration, and emulsification

Mona Kharazi*, Javad Saien, Morteza Torabi, Mohammad Ali Zolfigol

Faculty of Chemistry and Petroleum Science, Bu–Ali Sina University, Hamedan, 6517838695, Iran

ARTICLE INFO

Article history:
Received 19 February 2023
Received in revised form
22 June 2023
Accepted 10 July 2023
Available online 13 July 2023

Edited by Yan-Hua Sun

Keywords:
Tripodal ionic liquids
Green materials
Enhanced oil recovery
Interfacial tension
Wettability
Emulsification

ABSTRACT

Surface active ionic liquids (SAILs) are considered as prominent materials in enhanced oil recovery thanks to their high interfacial activity. This study reports the preparation and applications of a nanostructure Tripodal imidazolium SAIL as an environmentally-friendly substitute to the conventional surfactants. The product has a star-like molecular structure centered by a triazine spacer, namely $[(C_4im)_3TA][Cl_3]$, prepared by a one-step synthesis method and characterized with FT-IR, NMR, XRD, and SEM analysis methods. The interfacial tension of the system was decreased to about 78% at critical micelle concentration of less than 0.08 $mol \cdot dm^{-3}$. Increasing temperature, from 298.2 to 323.2 K, improved this capability. The solid surface wettability was changed from oil-wet to water-wet and 80% and 77% stable emulsions of crude oil–aqueous solutions were created after one day and one week, respectively. Compared to the Gemini kind homologous SAILs, the superior effects of the Tripodal SAIL were revealed and attributed to the strong hydrophobic branches in the molecule. The Frumkin adsorption isotherm precisely reproduced the generated IFT data, and accordingly, the adsorption and thermodynamic parameters were determined.

1. Introduction

Despite worldwide growing demand for energy, primary and secondary recoveries produce low percentages of crude oils from mature reservoirs (Tamayo-Mas et al., 2016). Accordingly, injection of surfactants for reducing crude oil–water interfacial tension (IFT), improving capillary number, altering rock wettability, and forming microemulsion have been attempted in different ways (Kharazi et al., 2022; Razzaghi-Koolaee et al., 2022; Painter et al., 2010). Meanwhile, the main challenge of conventional surfactants is to lose their performance in the harsh conditions of reservoirs and create environmental problems (Saien et al., 2022).

Surface active ionic liquids (SAILs), with amphiphilic nature and high stability show great potential for replacing conventional surfactants. SAILs, which exhibit advantages over thermal and chemical treatments, are resistive in brine solutions, non-flammable and recyclable (Hou et al., 2022; Zhou et al., 2016).

In view of environmental protection, unlike most conventional hazardous surfactants, most of the SAILs exhibit low toxicity, minor vapor pressure, and are environmentally friendly. These are documented according to the Classification Labelling and Packaging (CLP) or criteria of the Globally Harmonized System (GHS) regulations (Bera and Belhaj, 2016; de los Ríos et al., 2013). Meanwhile, the toxicity of SAILs can be tuned by an appropriate molecular design. For instance, use of the imidazolium SAIL with Cl anion is satisfactory in an enzyme-friendly environment (Liu et al., 2021). Biodegradation is also important in the field of green chemistry. In this regard, the proper biodegradability and mineralization of the imidazolium SAILs have been confirmed (Panchal et al., 2020). These advantages, as well as the high stability and recyclability of SAILs (Pal et al., 2019; Painter et al., 2010) are remarkable. Noteworthy, cationic SAILs, due to charge repulsion, are reluctant for adsorbing on the positive charge carbonate rocks which constitute about 60% of the world reservoirs (Joonaki et al., 2016).

Considering these features, multicationic SAILs (including Gemini and Tripodal types), consist of more than one cationic and anionic portions. Accordingly, they exhibit superior interfacial

* Corresponding author.
E-mail addresses: kharazi.mona@yahoo.com, m.kharazi@sci.basu.ac.ir (M. Kharazi).

https://doi.org/10.1016/j.petsci.2023.07.010

Abbreviates

CMC	Critical micelle concentration
EOR	Enhanced oil recovery
HLB	Hydrophilic-lipophilic balance
IFT	Interfacial tension
OF	Objective function
O/W	Oil-in-water emulsion
SAIL	Surface active ionic liquid
A	Interface area occupied by each molecule, m^2
b	Adsorption equilibrium constant, $dm^3 \cdot mol^{-1}$
C	Ionic liquid or electrolyte concentration, $mol \cdot dm^{-3}$
f	Ions average activity coefficient
G	Gibbs free energy, $kJ \cdot mol^{-1}$
N_{Av}	Avogadro's number
R	Universal ideal gas constant, $J \cdot mol^{-1} \cdot K^{-1}$
S	Entropy at the interface, $J \cdot K^{-1} \cdot m^{-2}$
U	Energy at the interface, $J \cdot m^{-2}$
T	Temperature, K

Greek symbols

β	Molecular interaction parameter
Γ	Interface excess concentration, $mol \cdot m^{-2}$
γ	Interfacial tension, $mN \cdot m^{-1}$
Δ	Difference
θ	Interface layer coverage or contact angle
π	Interfacial pressure, $mN \cdot m^{-1}$
ρ	Density, $kg \cdot m^{-3}$
ρ''	Water molar concentration, $mol \cdot dm^{-3}$

Subscripts

ads	Adsorption
cal	Calculated
exp	Experimental
F	Frumkin
m	Maximum or minimum
mic	Micellization
∘	Pure state

Superscript

∘	Standard state

activity of lower critical micelle concentration (CMC), easier emulsion formation, greater thermal and salinity resistance, and lower vapor pressure compared to monocationic branch SAILs (Saien et al., 2022; Ezzat et al., 2021). Adding to these, studies have confirmed that the stretched conformation of multicationic SAILs limit their penetration into cell membranes and give low hazards to organisms (Zhang et al., 2012). In this regard, Sharma et al. (2008), by synthesizing 28 symmetrical Tripodal SAILs and testing their ability in different aspects, reported that the physico-chemical properties of Tripodal SAILs were simply modified compared to traditional samples. Relevantly, Nacham et al. (2015) introduced two Tripodal imidazolium SAILs with higher surface activity in aqueous solutions and with lower CMC compared to single chain ones. Meanwhile, the nano-size SAIL particles improves their interfacial activity for better oil field operations (Pavia et al., 2014).

In this context and in the continuity of our previous studies (Kharazi et al., 2020, 2021; Saien et al., 2019), present work reports the results of a novel nano SAIL with prominent properties. The Tripodal imidazolium SAIL with a star-like molecular structure, namely [3,3′,3''-(1,3,5-triazine-2,4,6-triyl)tris(1-butyl-1H-imidazole-3-ium) chloride] abbreviated as $[(C_4im)_3TA][Cl_3]$, was synthesized and its structure was characterized by various methods. Worth mentioning, the lipophilicity as an important parameter in the toxicity of SALs (Steudte et al., 2014); i.e. the longer the alkyl chain, the more probable entering the SAILs to the cells of organisms, causing membrane damage and cell damage (Kapitanov et al., 2019). Thus, a short alkyl chain (four carbons) Tripodal SAIL was preferred. The important effects in IFT and CMC reduction, wettability alteration and emulsification of crude oil–water system were explored. The effect of temperature was also considered. In theoretical study, the Frumkin adsorption isotherm was used to reproduce the experimental data and to obtain the thermodynamic and relevant parameters. For better demonstrating, the results are compared with the previously examined homolog structure Gemini SAILs. Synthesis of this nanostructure Tripodal SAIL and its application for different aspects of EOR have not been previously reported.

2. Experimental

2.1. Materials

The crude oil was obtained from an Iran southern oil field. Details of the specification and the composition of the crude oil are listed in Table 1. Purity (mass fraction) and the supplier of the other chemicals for synthetizing the SAIL are listed in Table 2. The chemicals were analytical grade and were utilized with no purification. Freshly deionized water (conductivity less than 0.07 $\mu S \cdot cm^{-1}$) was used to prepare solutions of the SAIL.

2.2. Synthesis and characterization of the Tripodal SAIL

2.2.1. Synthesis

In a number of imidazolium based SAILs, benzene ring has been as the spacer in the molecular structure; however, it is attempted in this study to design a Tripodal SAIL with triazine moiety spacer. The synthesis procedure is shown in Scheme 1. Briefly, 40 mmol (4.96 g) of 1-butyl imidazole was dissolved in 30 cm^3 toluene. In another

Table 1
Principle specifications and compositions of the used crude oil.

Specification/composition	Value
Saturated, wt%	54.0
Aromatic, wt%	22.3
Resin, wt%	6.7
Asphalt, wt%	7.7
Acidity number, mg KOH/g	0.09
Sulphur content, wt%	1.63
Salt, lbs per 1000 bbls	4
Water content, wt%	Nil
°API	20.7
Density at 20 °C, $g \cdot cm^{-3}$	0.915
Pour point, °F	10
Flashpoint, °F	70
Reid vapor pressure, psi	12.1
Viscosity at 70 °F, cP	55
Viscosityat 100 °F, cP	44
Kinematic viscosity at 70 °F, cSt	60
Loss at 200 °C, wt%	9.3

Table 2
Purity (mass fraction) and supplier of the used materials other than crude oil.

Material	Purity (mass fraction)	Supplier
Cyanuric chloride	>0.98	Merck
1-butylimidazole	>0.98	Merck
Toluene	>0.99	Merck
n-hexane	0.99	Exir
Ethanol	0.96	Merck

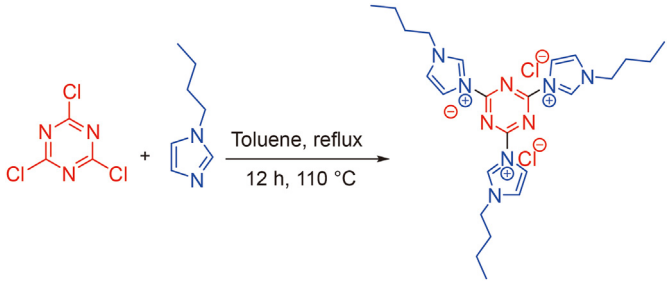

Scheme 1. The procedure of the $[(C_4im)_3TA][Cl_3]$ synthesizing route.

solution, 10 mmol (1.84 g) cyanuric chloride was dissolved in toluene (30 cm^3) in a 100 cm^3 round-bottomed flask. Then the solution of 1-butyl imidazole was added to the cyanuric chloride solution dropwise. The provided reaction mixture was refluxed for 12 h at 110 °C to complete the reaction. In this way, C–Cl bonds of cyanuric chloride were broken by the attack of 1-butylimidazole and consequently the Tripodal SAIL was synthesized containing the chloride ions. The obtained precipitated product was filtered and washed three times with *n*-hexane, once with cold ethanol and finally dried at 50 °C to give the pure product of [3,3′,3″-(1,3,5-triazine-2,4,6-triyl)tris(1-butyl-1H-imidazole-3-ium) chloride], abbreviated as $[(C_4im)_3TA][Cl_3]$. As observed, the hydrophobic parts of the Tripodal SAIL are composed of three alkyl chains and a triazine spacer, but the hydrophilic parts are of three imidazolium rings. Accordingly, the hydrophilic-lipophilic balance (HLB) (Pillai and Mandal, 2022) of the Tripodal SAIL was calculated as 8.93 indicating a water-soluble surfactant with high wetting and spreading efficiency as well as the ability to form O/W emulsions.

A main challenge in the SAIL applications is their cost, which inevitably limits their utilization in large-scales. Generally, price of raw materials has the major contribution in this regard. Here inexpensive and commercially available raw materials (listed in Table 2) with high purity and reactivity were used for preparing the Tripodal SAIL.

2.2.2. Characterization

According to FT-IR spectrum, shown in Fig. S1 (Supplementary data), the stretching vibration of aliphatic C–H groups are appeared within 2959–2782 cm^{-1}, which are relevant to butyl chains. The stretching vibration of aromatic C–H groups, appeared at about 3036 cm^{-1} is relevant to imidazolium rings. The sharp peaks in the areas of 1725 and 1622 cm^{-1} are related to C=N and C=C groups, respectively (Pavia et al., 2014).

^1H NMR and ^{13}C NMR analyses help to accurate detecting the product structure as well as confirming its purity. As can be seen in ^1H NMR spectrum (Fig. S2(a)), the existence of a triplet pick with integral of nine in 0.86 ppm verify the terminal methyl groups of butyl chains. Three methylene groups with integrals of about six are appeared at 1.20, 1.75, and 4.24 ppm, respectively. Due to the high electronegativity of nitrogen compared to carbon, the methylene linked to nitrogen undergoes a higher chemical shift at 4.24 ppm. Imidazolium ring hydrogens are also appeared at 7.70, 7.88, and 9.36 ppm. Further, ^{13}C NMR confirms the accuracy and purity of the synthetized Tripodal SAIL. One peak at 150.40 ppm is related to triazine ring and three peaks at 135.44, 122.43, and 120.11 ppm are related to imidazolium rings. The peaks of aliphatic carbons of butyl chains are properly displayed at 48.63, 31.91, 19.26, and 13.71 ppm (Fig. S2(b)).

According to the sharpness of the XRD peaks (Fig. S3)., the synthetized Tripodal SAIL has relatively good crystal structure with diffraction lines at $2\theta = 13.34°, 17.34°, 18.54°, 20.14°, 20.89°, 22.04°, 27.89°$, and 28.24°. The Scherrer equation, $D = K\lambda/(\beta\cos\theta)$, in which K and λ are the constants and the X-ray wavelength, β is the full width at the half maximum of the peak in radians, and θ is to the Bragg diffraction angle, could be used. Accordingly, the crystalline size of the product is obtained within 21.3–24.5 nm. Details are provided in the Table S1.

The provided SEM image (Fig. 1) represents the morphology of the product, which shows spherical particles with almost uniform distribution and apparent nanometer size of 60.6–91.4 nm. Based on investigations, nano-size surfactants show superior performance in adsorption, micelle formation, and emulsification compared to conventional surfactants (Gbadamosi et al., 2018; Jiang et al., 2018). Noteworthy, the injection of nano-size materials (here, the Tripodal SAIL), strongly prevents the crude oil backflow, helps to separating oil drops from rocks and inhibits the asphaltene deposition (Łuczak et al., 2016). Further, the higher viscosity of these solutions can increase the oil displacement as well as sweeping efficiency (Gbadamosi et al., 2018; Jiang et al., 2018).

Dynamic light scattering (DLS) analysis was also employed to determine the size of particles and their aggregates in aqueous solutions. For this purpose, solutions with 1×10^{-3} mol·dm^{-3} (less than CMC) and with 0.1 mol·dm^{-3} (more than CMC) were used. The measured values, known as "hydrodynamic size" were within 4.8–23.2 nm for the particles and stayed within 564.9–2317.6 nm for the micelles. The corresponding spectra is presented in Fig. 2.

2.3. Instruments and measurements

The IFT and contact angle between crude oil–aqueous solutions of the Tripodal SAIL, were measured by means of a pendant drop tensiometer (Fars EOR Technol, CA-ES10 model). This measurement is based on the formation of crude oil drops at the tip of different stainless steel needles dipped in the aqueous phase. The details of the set-up and method have already been described (Kharazi et al., 2019; Saien et al., 2019). The tensiometer can determine the IFT (γ) by automatically analyzing the formed droplets shape by image processing system and calculating a balance between buoyancy and interfacial forces according to (Stauffer, 1965):

$$\gamma = \frac{\Delta\rho g D^2}{H} \quad (1)$$

where g and D are, respectively, the gravitational constant and the equatorial diameter. Also, $\Delta\rho$ and H are the difference of the aqueous and crude oil densities as well as the drop shape parameter that depends according to a polynomial correlation as a function of shape factor of $S = d/D$, where d is the diameter at distance D from top of the drop.

Using this set-up, crude oil–pure water equilibrium IFT was detected as 31.8 mN·m^{-1} at 298.2 K. For more validation, the pure water–air IFT was measured as 71.9 mN·m^{-1} at 298.2 K, which was close to 72.0 mN·m^{-1}, reported in the literature (Lan et al., 2016). To ensure consistency, each measurement was repeated at least twice. Table S2 lists details of the achieved data. All the measurements, under a certain SAIL concentration, were examined under ambient

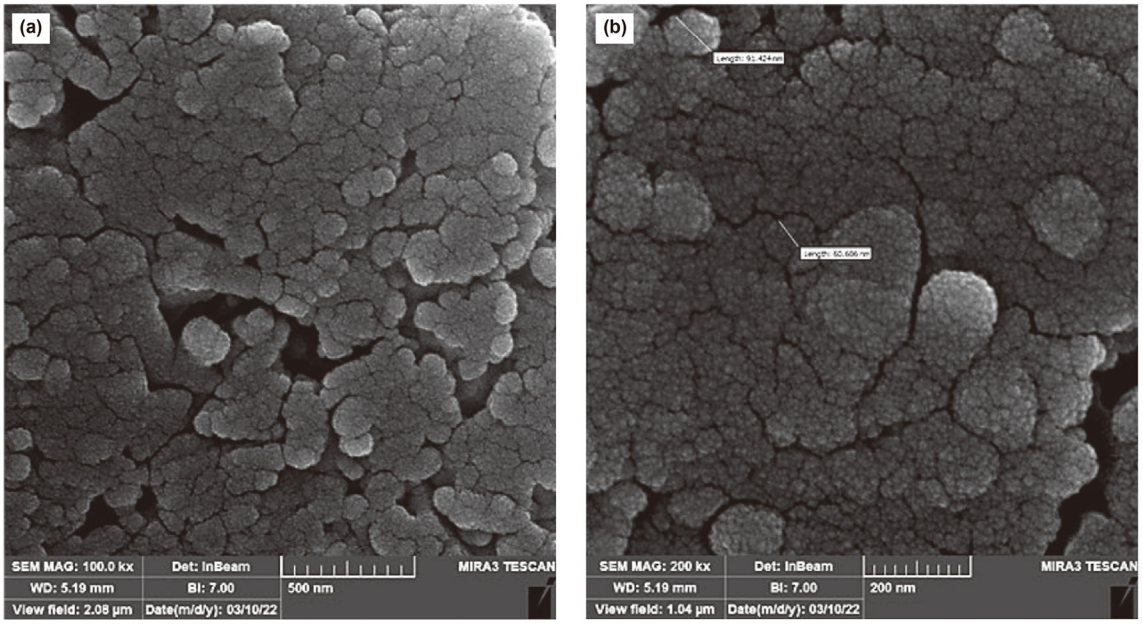

Fig. 1. The SEM images of the synthesized SAIL with low (**a**) and high (**b**) magnifications.

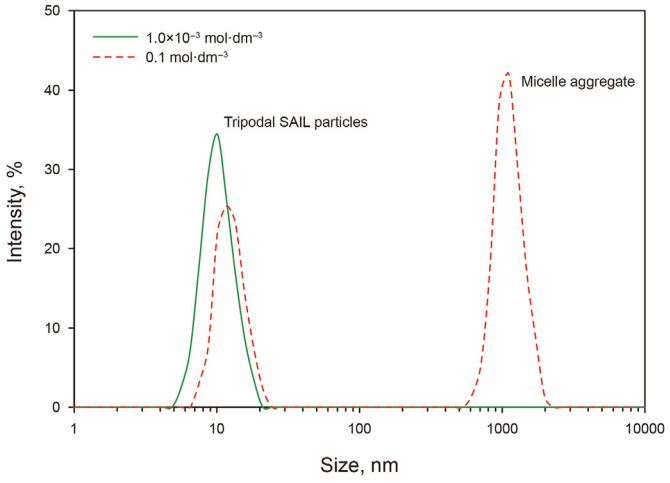

Fig. 2. The DLS spectra of the $[(C_4im)_3TA][Cl_3]$ product at lower and higher concentrations than CMC.

pressure, and at four temperatures within 298.2–328.2 K adjusted with a temperature sensor (PT 100, uncertainty 0.1 K) and fine tunable electric heater. At each temperature, the CMCs were graphically determined from the intersection of the upper and lower tangential lines of the breakpoint region in the IFT against the SAIL concentration graphs.

Prior to experiments, various aqueous solutions of the Tripodal SAIL in the range of 1.0×10^{-4} –0.2 mol·dm^{-3} were prepared by mass. For this purpose, SAIL was weighed up using a 1.0×10^{-4} g uncertainty Ohaus balance (Adventurer Pro, AV 264). It is important to note that the used SAIL solutions could be reused many times without significant change in their impact. At each temperature, the density of solutions was detected using an oscillating U-tube densitometer (Anton Paar DMA 4500, uncertainty 1.0×10^{-4} g·cm^{-3}) with automatic viscosity correction.

For measuring the contact angles, a quartz sheet was first immersed in the crude oil. The system was left overnight (14–18 h) for aging to approach the real reservoir condition. After that, crude oil was injected through a needle in the aqueous phase with a certain concentration to release a drop to attach the top quartz surface in the cell (Kharazi et al., 2023). After at least 1 h, the image of the crude oil drop was captured and the contact angle was determined by analyzing the geometry (with the aid of an image processing system) of the hemisphere crude oil drop surrounded by an aqueous solution. Noteworthy, the mean contact angles between the left and right sides was determined automatically.

To evaluate the capability of emulsion formation, equal volumes of 2 cm^3 from the crude oil and the aqueous solution of the Tripodal SAIL with a typical concentration of 0.01 mol·dm^{-3} (corresponding to a middle IFT) were transferred to the glass vials and sonicated by using a SONICA 2400ETH S3, 40 kHz, 305 W ultrasound bath for 30 min. After resting for one day and one week at 298.2 K, the corresponding emulsion indices were easily obtained from $V_e/V_t \times 100\%$ in which V_e and V_t, stand for the emulsion and the total sample volumes. The emulsion microscopic images were also taken to observe the dispersion of droplets on the glass lames using an Olympus BX-60 loupe microscope (45 × magnification).

3. Results and discussion

3.1. IFT variation

The crude oil–water IFT variations against the Tripodal SAIL concentration is shown in Fig. 3. As is apparent, presence of the SAIL till CMC, at which drastic declines in IFT appeared as 7.2 and 6.4 mN·m^{-1} (maximum reductions of 77.4% and 78.5%) at temperatures of 298.2 and 328.2 K, respectively. This is desired in EOR processes with respect to increasing the capillary number in the reservoirs (Zhang et al., 2009). An economically attractive result is reducing more than 50% in IFT with a surfactant concentration of less than 0.01 mol·dm^{-3} (Rosen et al., 2005), precisely attained here. Upon reaching CMC of the Tripodal SAIL, at concentrations below 0.08 mol·dm^{-3}, the adsorbed particles saturate the interface. At this point, the IFT remains nearly constant. For a better clarification, all the related values at different temperatures are listed in Table 3.

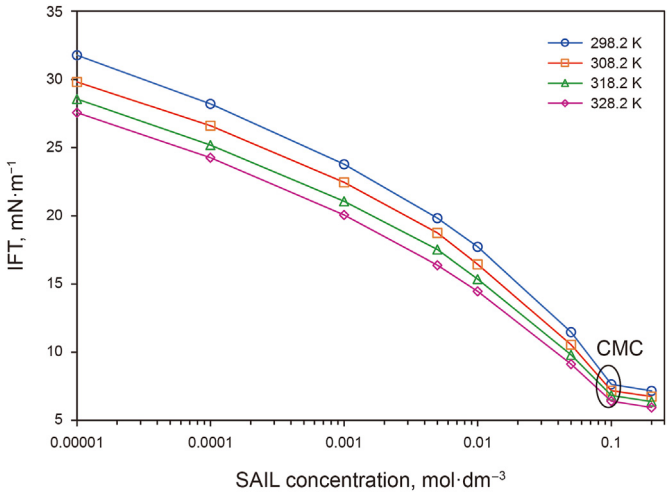

Fig. 3. IFT variations as a function of the Tripodal SAIL concentration at different temperatures.

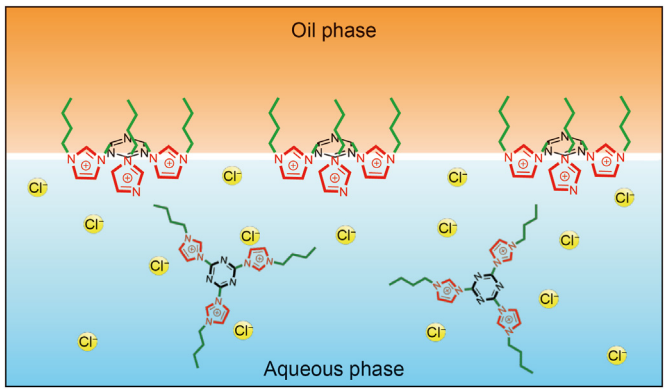

Fig. 4. A schematic of Tripodal SAIL configuration in the crude oil–water system.

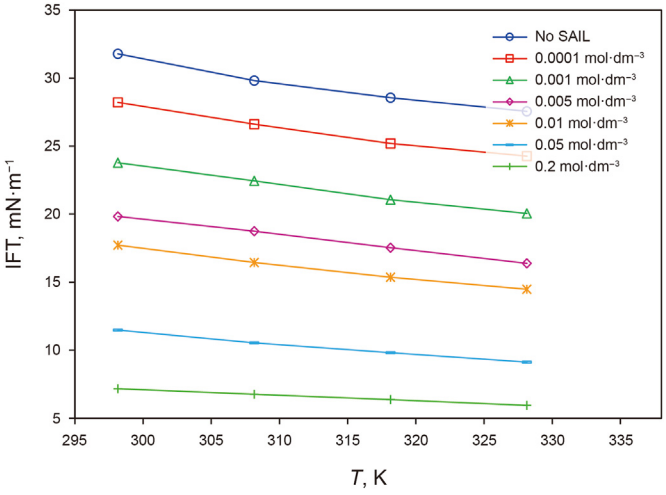

Fig. 5. IFT variation versus temperature for different Tripodal SAIL concentrations.

The amazing effect in IFT reduction is corresponding to the strong amphiphilic nature of the Tripodal SAIL, which creates a high migration tendency toward the oil–water interface. Under this situation, the hydrophobic parts, containing the side chains and the aromatic spacer ring, are placed in the crude oil phase at the interface, whereas, the hydrophilic ring with the charged nitrogen atoms place in the aqueous phase (Saien et al., 2015; Gao and Sharma, 2013a). With this configuration, as shown schematically in Fig. 4, SAIL particles find the lowest free energy and the intermolecular forces diminish, bringing about high IFT reductions. It is worth to note that electrostatic repulsion inhibits a close orientation at the interface when a single chain SAIL (with the same chain length) is used; however, the spacer ring in the Tripodal SAIL compensates the electrostatic repulsion, giving a closer packing and significant IFT reduction (Kharazi et al., 2022).

In EOR, surfactants are inevitably imposed to high dominant temperatures in reservoirs. Here, results show that temperature gives extra IFT reductions under certain concentrations of the SAIL (Fig. 5). The highest decrease was about 20.5% compared to IFT at 298.2 K, for 5.0×10^{-2} mol·dm^{-3}. Therefore, performance and stability of the Tripodal SAIL is improved with temperature. IFT reductions due to temperature effect can be ascribed with the following causes (Saien et al., 2023):

- Interrupting the water molecules surrounding the hydrophilic parts of Tripodal SAIL, which reduces their solubility in the aqueous phase and facilitates their adsorption.
- Improving molecular movements which weakens the intermolecular forces at the interface.
- Reducing the viscosity of the aqueous phase, giving in turn, a higher mass transfer rate from bulk to the subsurface and SAIL adsorption at the interface.

In the same way, decomposition of water icebergs around the SAIL particles diminishes the CMCs (Table 3). Under these conditions, alkyl chains tend more to aggregate at low concentrations (Chen et al., 2018). Thus, from CMC point of view, higher temperatures are also desired.

3.2. Wettability alteration

Wettability reflects the interaction between the brine and crude oil in contact with the reservoir rock. This is known as an essential parameter for controlling the remaining original oil in place (OOIP). In wettability alteration, the mobility of the crude oil increases by transforming the rocks from oil-wet to water-wet, which causes the residual oil easily detached from rocks, leading to significant EOR (Pillai and Mandal, 2019). Wettability could be assessed with the contact angle of liquids with a surface. In the crude oil–water–rock system, surface of reservoirs are categorized as hydrophilic (water-wet) with a contact angle of 0–80°, moderate (intermediate-wet)

Table 3
The obtained empirical parameters for the TSAIL.

Temperature, K	Crude oil–water IFT $\gamma_{\circ}$, mN·m^{-1}	CMC, mol·dm^{-3}	IFT at CMC γ_{CMC}, mN·m^{-1}	Minimum IFT γ_{min}, mN·m^{-1}	Maximum IFT reduction, %
298.2	31.8	8.8×10^{-2}	7.6	7.2	77.4
308.2	29.8	8.4×10^{-2}	7.2	6.8	77.5
318.2	28.6	7.9×10^{-2}	6.8	6.4	77.7
328.2	27.6	7.5×10^{-2}	6.4	5.9	78.5

with a contact angle of 80°–100°, and hydrophobic (oil-wet) with a contact angle of 100°–180° (He et al., 2015). It should be noted that for an oil drop forming in an aqueous phase, the external contact angle surrounded by the aqueous phase is deliberated.

The appeared shape of attached drops, surrounded by each of the Tripodal SAIL solutions are presented in Fig. 6(a) and the corresponding contact angles of crude oil drops, measured at the 298.2 K, in Fig. 6(b). As observed, the contact angle of 156.3° is highly decreased to 31.4°, with, the 0.2 mol·dm^{-3} SAIL concentration. Thus, in addition to the previous mentioned advances, the Tripodal SAIL can remarkably change the wettability.

The proposed mechanism for this observation is that the Tripodal SAIL, could accumulate on both the crude oil drops and on the solid surface so that the alkyl chains direct toward the plates surface and the polar parts toward the solution. This configuration hydrophilizes the plates; thus, oil separation happens and the oil-wet surface changes to water-wet, rising with the SAIL concentration (Gbadamosi et al., 2019).

3.3. Emulsifying capability

During crude oil recycling, it is necessary to transfer surfactants to zones with low permeability and dissolve the remaining crude oils by forming stable oil-in-water (O/W) or multiple emulsions. Noteworthy, forming emulsions diminishes the adsorption of crude oils on the reservoir rocks and thus, facilitates the movement of the residual crude oils (Guang et al., 2018). Emulsions also facilitate injected fluids to flow in non-swept areas, block permeable pathways to inhibit the backflow of crude oil and highly improve the mobility and the sweeping efficiency (Kumar and Mandal, 2018; Yazhou et al., 2017). Indeed, a low IFT is a basic requirement for stable emulsions. Notably, creating stable emulsions with conventional surfactants is often available with the aid of co-surfactants, which are often volatile and involve an environmental risk. In this sense, due to powerful cohesive forces, SAILs can make stable emulsions with no co-surfactant requirement (Bera and Belhaj, 2016).

The photographs of the crude oil–water emulsions with no SAIL and with typical 0.01 mol·dm^{-3} of the Tripodal SAIL after one day and one week, as well as their microscopic images are shown in Fig. 7. As is obvious, no emulsion was created with pure water; but, stable emulsions were corresponding in the presence of the SAIL. Emulsification indices as high as 80.5% and 76.6% were, respectively, achieved after one day and one week, implying that the used SAIL is a proper candidate for EOR. Furthermore, the prepared emulsions were monitored after three months and the stability of emulsions was observed. Similarly, from microscopic images it is clear that the presence of SAILs leads to forming crude oil droplets in water. This is because of the strong amphiphilic nature of the SAIL, giving directional adsorption at the interface of droplets and forming protective films which facilitate dispersion of the crude oil in the aqueous media (Gao and Sharma, 2013a, 2013b).

4. Theoretical consideration

The well-known Frumkin adsorption isotherm, was satisfactorily fitted to the experimental IFT data at concentrations below CMC under examined temperatures. This isotherm emphasizes on existing non-ideal interactions (attraction or repulsion) between adsorbed particles at an interfaces (Birdi, 2009). Given the three positively charged aromatic rings that provides strong interfacial interactions between the Tripodal SAILs, this isotherm looks

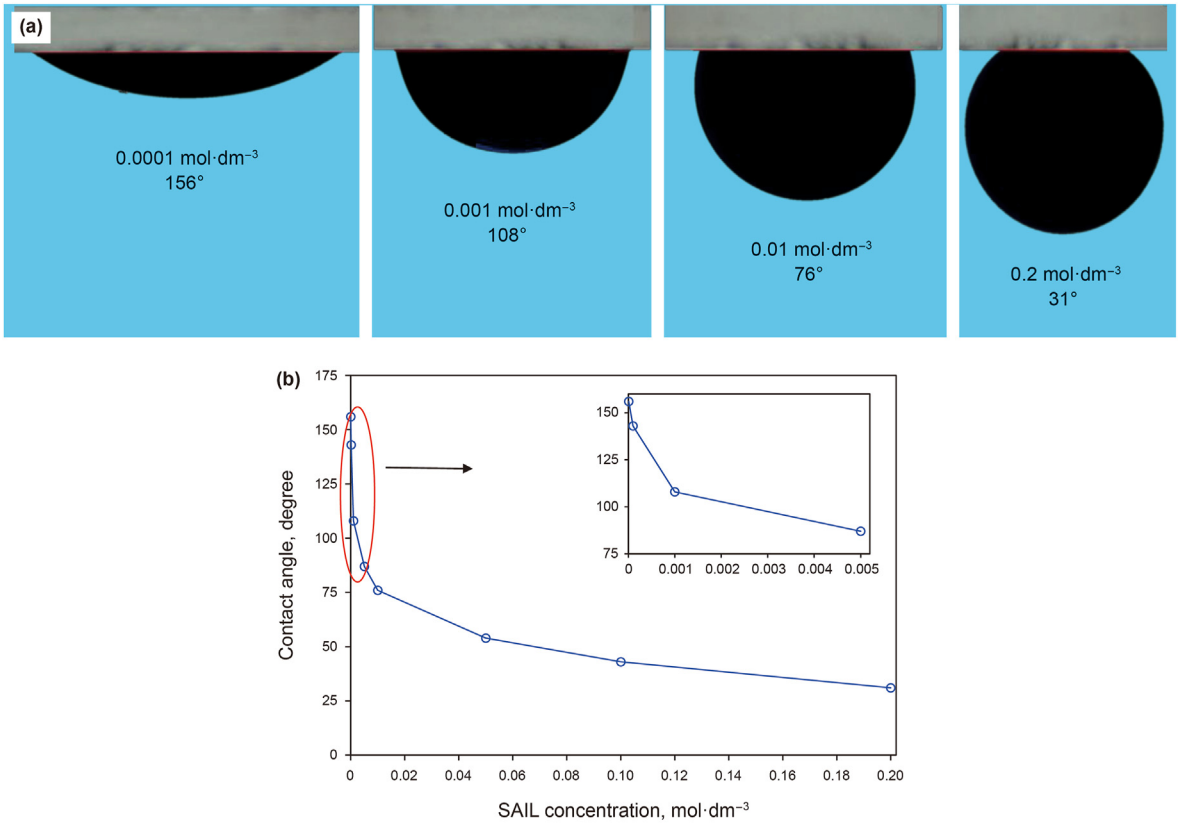

Fig. 6. The shapes of the crude oil drops under different Tripodal SAIL aqueous solutions (**a**), and the contact angles of crude oil drops, surrounded with Tripodal SAIL solutions, on the quartz surface (**b**), all at 298.2 K.

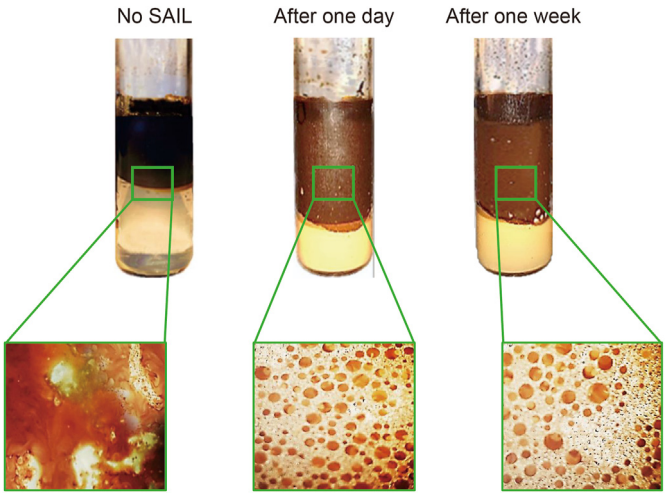

Fig. 7. The crude oil–water emulsions and their microscopic images (45 × magnification) with no SAIL and with 0.01 mol·dm^{-3} of the Tripodal SAIL after one day and one week.

adaptable to the data. The equation of state and the isotherm are defined by the following equations (Stubenrauch et al., 2005):

$$\Pi = -2RT\Gamma_{m,F}\left[\ln(1-\theta)+\beta\theta^2\right] \tag{2}$$

$$b_F\, f_{\pm}\left[C\left(C+C_{electrolyte}\right)\right]^{1/2} = \frac{\theta}{1-\theta}\exp(-n\beta\theta) \tag{3}$$

In these equations, $\Pi = \gamma_\circ - \gamma$, known as the interfacial pressure, is the difference between clean system IFT, $\gamma_\circ$, and the present IFT, γ. Based on the Gibbs dividing interface theory on which Frumkin isotherm is based, n is related to the number of cations and anions of the ionic surface-active substance after dissociating at the electro-neutral interface (Stubenrauch et al., 2005). Moreover, R and $\Gamma_{m,F}$, are the universal gas constant and the maximum interface excess concentration related to Frumkin model which represents the adsorption effectiveness. Moreover, $\theta = \Gamma/\Gamma_{m,F}$ displays the interface layer coverage, b_F shows the Frumkin adsorption constant, which describes adsorption tendency and β indicates the van der Waals molecular interaction parameter in which positive and negative values are relevant to attractive and repulsive interactions (Stubenrauch et al., 2005). Other parameters are $f_{\pm}$, as the activity coefficient of ions that is approaching to unit at low concentrations, and, C and $C_{electrolyte}$ as the bulk concentration of a surface-active substance and a salt (if present). Fittings the experimental data with the Frumkin isotherm was attained by reaching a low value of the objective function (OF), defined as (Möbius et al., 2001):

$$OF = \sum_{i=1}^{m}\frac{\Delta C_i}{C_{exp,i}}\frac{\Delta\Pi_i}{\Pi_m - \Pi_1} \tag{4}$$

in which the term $\Delta C_i = |C_{exp,i} - C_{cal,i}|$ and $\Delta\Pi_i = (\Pi_{exp,i+1} - \Pi_{exp,i-1})/2$, respectively, indicate the difference of concentrations (experimental and calculated) as well as interfacial pressure values relevant to the ith data point. Also, $\Pi_m = \gamma_\circ - \gamma_m$ represents the maximum interfacial pressure corresponding to γ_m of the last IFT in a series with m data points. As shown in Fig. S4, the Frumkin adsorption isotherm is adaptable to the data. Accordingly, the appropriate parameters and the objective function, OF, for different temperatures are listed in Table 4.

As can be seen, $\Gamma_{m,F}$ increases with temperature, atributed to improving the thermal mobility of the SAIL particles in addition to dehydration of hydrophobic parts of the SAIL as was described in Section 3.1. Conversely, the Frumkin adsorption equilibrium constant, b_F, decreases as temperature increases. It is because of the more compact interface arrangement of adsorbed particles, which leads to greater electrostatic repulsion. Rising mobility of particles at the interface decreases the adsorption tendency at high temperatures. The negative values of the molecular interaction parameter, β, confirms electrostatic repulsion among the adsorbed Tripodal SAILs with positively charged head groups. As a result, the more adsorbed particles at elevated temperatures provides a greater electrostatic repulsion. According to these, the minimum interface area occupied by each molecule, A_m can be calculated from:

$$A_m = \frac{1}{\Gamma_{m,F}N_{Av}} \tag{5}$$

where N_{Av} displays the Avogadro's number. Reasonably, temperature increases the interface concentration and causes compact orientation of particles at the adsorption layer, and reduces the occupied area by each molecule. Finally, considering the temperature range, the OF values were within 6.2×10^{-2}–8.2×10^{-2} that approves proper fittings.

The thermodynamic parameters of ΔG°_{ads} and ΔG°_{mic}, relevant to adsorption and micellization Gibbs free energies, which, reflect the adsorption and aggregation tendencies were calculated by (Liu et al., 2012; Möbius et al., 2001):

$$\Delta G^{\circ}_{ads} = -2RT\ln\left(\frac{b_F\rho'}{2}\right) \tag{6}$$

$$\Delta G^{\circ}_{mic} = RT\ln C_{CMC} \tag{7}$$

where $\rho' = \rho/18$ is the water molar concentration. As presented in Table 5, these energies, confirm that Tripodal SAIL adsorption at the crude oil–water interface, and micellization in the bulk are spontaneous. At high temperatures, the thermal agitation of adsorbed particles elevates, decreasing the absolute free energy of adsorption. Meanwhile, dehydration of the hydrophobic parts of the SAIL in the balk phase, improves the aggregation tendency with temperature. As another point, the absolute values of ΔG°_{ads} are significantly higher than ΔG°_{mic}, meaning that the Tripodal SAIL tends to rather adsorb rather than remain in the bulk and form aggregate.

Finally, the interface entropy change, ΔS, as well as the energy change, ΔU, can be obtained from (Motomura et al., 1982):

$$\Delta S = -\left(\frac{\partial\gamma}{\partial T}\right)_{p,C} \tag{8}$$

$$\Delta U = \gamma + T\Delta S \tag{9}$$

The variations of ΔS and ΔU versus temperature are illustrated in Figs. S5 and S6. The variations of ΔS with temperature is due to the involved competitive phenomena of improving agitation of particles and dehydration of hydrophobic parts of SAILs at the interface (Asadabadi et al., 2013). The former causes entropy rising and the latter creates a strong van der Waals attraction between the hydrophobic parts of the SAIL with low entropy values (Matsubara et al., 2010). Due to the dependency on ΔS, a similar variation trend is observed for the energy ΔU.

Table 4
The theoretical parameters obtained from the Frumkin adsorption isotherm at different temperatures.

Temperature T, K	Maximum interface excess concentration $\Gamma_{m,F}$, mol·m^{-2}	Frumkin adsorption equilibrium constant b_F, dm^3·mol^{-1}	Molecular interaction parameter β	Minimum interface area occupied by each molecule A_m, m^2	Objective function
298.2	1.3×10^{-6}	550	−3.8	8.7×10^{-36}	6.2×10^{-2}
308.2	1.5×10^{-6}	350	−4.4	7.3×10^{-36}	7.1×10^{-2}
318.2	1.7×10^{-6}	275	−5.1	6.1×10^{-36}	6.6×10^{-2}
328.2	1.9×10^{-6}	250	−5.6	4.9×10^{-36}	8.2×10^{-2}

Table 5
The water molar concentration and free energies of adsorption and micellization at different temperatures.

Temperature T, K	Molar concentration of water ρ', mol·dm^{-3}	Gibbs free energy of adsorption ΔG°_{ads}, kJ·mol^{-1}	Gibbs free energy of micellization ΔG°_{mic}, kJ·mol^{-1}
298.2	55.4	−46.5	−10.2
308.2	55.2	−46.8	−10.9
318.2	54.9	−47.5	−11.8
328.2	54.5	−48.5	−12.8

5. Comparative study

The performance of the Tripodal SAIL could be scrutinized by comparing with the previously investigated similar head group and alkyl chain length Gemini SAILs, i.e. [C$_4$im-C$_n$-imC$_4$][Br]$_2$, n = 2, 4 and 6 (Kharazi and Saien, 2022a). The crude oil–water IFT variations with concentration are shown in Fig. 8 at a typical temperature of 298.2 K. As it is possible to see, the nano Tripodal SAIL gives significantly higher IFT reductions even at lower concentrations, which is economically attractive in EOR. To reach a certain IFT, for instance15 mN·m^{-1}, the required amount of the Tripodal SAIL is only about 0.02 mol·dm^{-3}, whereas much higher concentrations, 0.5 to 0.7 mol·dm^{-3}, of the Gemini SAILs are required. Thus, it reveals that the three hydrophobic branches as well as the more hydrophobic aromatic spacer group give so effective capability to the Tripodal SAIL. Also, the spacer ring reduces better the electrostatic repulsion between charged head groups and provides easier adsorption (Kharazi and Saien, 2022b). This is confirmed by the found lower van der Waals molecular interaction, β, values of the Tripodal SAIL compared to that of the Gemini SAIL (see Table S3). A comparison of the $\Gamma_{m,F}$ values in this table, verifies the above results.

As shown in Fig. 9, drastically low CMCs are relevant to the Tripodal SAIL, giving average 89%, 91%, and 90% lower values than the Gemini SAILs with n = 2, 4, and 6, respectively. As previously pointed, more hydrophobicity and less electrostatic repulsion brings about so great aggregation tendency for the Tripodal SAIL. This also confirms the higher negative values of the free energy of micellization ΔG°_{mic} for the used SAIL (Table S3).

The Tripodal SAIL also presents greater emulsification

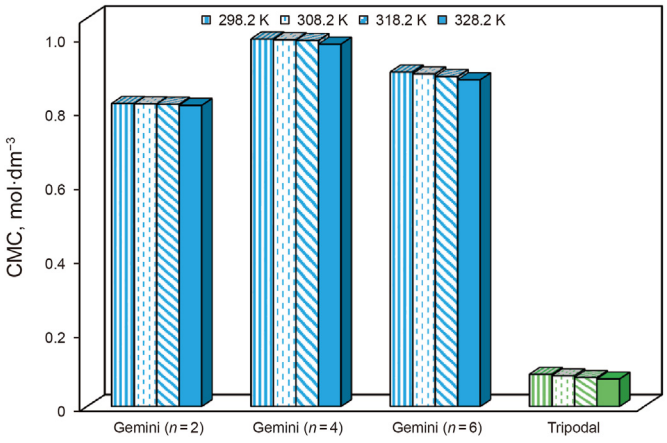

Fig. 9. Comparison of CMC values of the used Tripodal SAIL with different Gemini SAILs for the crude oil–water system at different temperatures.

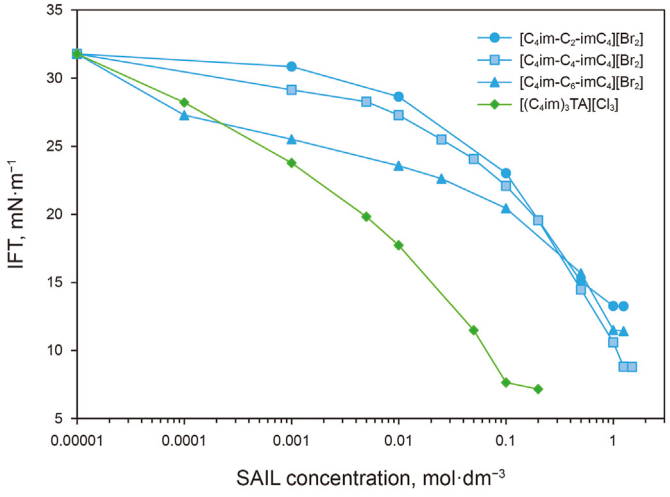

Fig. 8. Comparison of IFT variations of the used Tripodal with Gemini SAILs at 298.2 K.

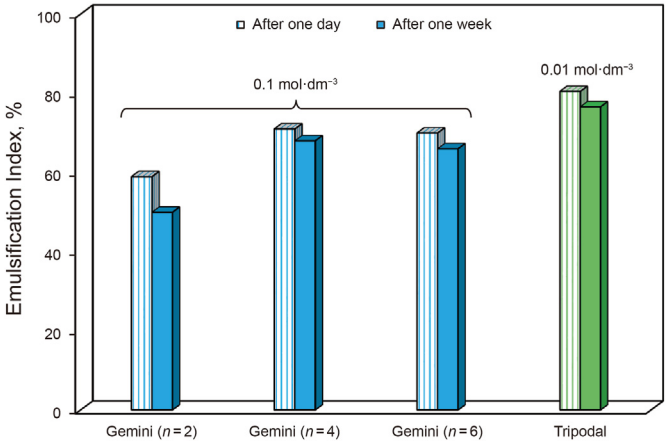

Fig. 10. The emulsification indices for 0.01 mol·dm^{-3} of the Tripodal and 0.1 mol·dm^{-3} of the Gemini SAILs after one day and one week, all at 298.2 K.

performance. Fig. 10 shows the emulsification indices for 0.01 and 0.1 mol·dm^{-3} (corresponded to a middle IFT) of the Tripodal and the Gemini SAILs, respectively. The data approve the Tripodal SAIL promising emulsifying capability at one order of magnitudes lower concentration, which is due to greater hydrophobicity and less electrical repulsion.

6. Conclusions

This study demonstrated the performance of a synthetized nano Tripodal SAIL with a star-like molecular structure in reducing the IFT and CMC as well as wettability alteration and emulsification of the crude oil–water system.

The outcomes revealed that thanks to its unique structure, the Tripodal SAIL could considerably decrease the crude oil–water IFT to about 78% at very low CMC and temperature favors the performance. Moreover, the surface wettability was easily transferred from oil-wet to water-wet as a consequence of diminishing adhesion between the crude oil and the surface. Adding to these, emulsification of crude oil–aqueous solutions revealed that the used SAIL could disperse the crude oil droplets in the aqueous phase and give stable emulsions. Compared to the Gemini SAILs, the superior performance of the used Tripodal SAIL in reducing IFT and CMC as well as increasing emulsification was revealed. These was observed at extremely lower concentrations, credited to the strong hydrophobicity of the three branches and presence of an aromatic spacer ring in the molecular structure.

In theoretical study, Frumkin adsorption isotherm was utilized for precisely fitting the experimental data and determining the related factors as well as the consistent thermodynamic parameters.

Briefly, the results concluded that the nano Tripodal SAIL could be considered as a desired and environmentally-friendly alternative in enhancing interfacial properties of the crude oil–water system. However, their actions in large scales have to be investigated to find operational problems.

Declaration of competing interest

The authors declare that they have no known competing financial interests or personal relationships that could have appeared to influence the work reported in this paper.

Acknowledgments

The authors would like to acknowledge the Bu Ali Sina University and the Iran National Science Foundation: INSF, under Grant number of 99031559, for their financial supports.

Appendix A. Supplementary data

Supplementary data to this article can be found online at https://doi.org/10.1016/j.petsci.2023.07.010.

References

Asadabadi, S., Saien, J., Khakizadeh, V., 2013. Interface adsorption and micelle formation of ionic liquid 1-hexyl-3-methylimidazolium chloride in the toluene+water system. J. Chem. Thermodyn. 62, 92–97. https://doi.org/10.1016/j.jct.2013.03.004.

Bera, A., Belhaj, H., 2016. Ionic liquids as alternatives of surfactants in enhanced oil recovery a state-of-the-art review. J. Mol. Liq. 224, 177–188. https://doi.org/10.1016/j.molliq.2016.09.105.

Birdi, K.S., 2009. Surface and Colloid Chemistry: Principles and Applications. CRC Press.

Chen, C., Wang, S., Kadhum, M.J., Harwell, J.H., Shiau, B.J., 2018. Using carbonaceous nanoparticles as surfactant carrier in enhanced oil recovery: a laboratory study. Fuel 222, 561–568. https://doi.org/10.1016/j.fuel.2018.03.002.

de los Ríos, A.P., Irabien, A., Hollmann, F., Fernández, F.J.H., 2013. Ionic liquids: green solvents for chemical processing. J. Chem. https://doi.org/10.1155/2013/402172, 2013.

Ezzat, A., Ayman, O., Atta, M., Al-Lohedan, H.A., 2021. Demulsification of stable seawater/Arabian heavy crude oil emulsions using star-like tricationic pyridinium ionic liquids. Fuel 304, 121436. https://doi.org/10.1016/j.fuel.2021.121436.

Gao, B., Sharma, M.M., 2013a. A family of alkyl sulfate gemini surfactants. 1. Characterization of surface properties. J. Colloid Interface Sci. 404, 80–84. https://doi.org/10.1016/j.jcis.2013.04.043.

Gao, B., Sharma, M.M., 2013b. A family of alkyl sulfate gemini surfactants. 2. Water–oil interfacial tension reduction. J. Colloid Interface Sci. 407, 375–381. https://doi.org/10.1016/j.jcis.2013.06.066.

Gbadamosi, A.O., Junin, R., Manan, M.A., Yekeen, N., Agi, A., Oseh, J.O., 2018. Recent advances and prospects in polymeric nanofluids application for enhanced oil recovery. J. Ind. Eng. Chem. 66, 1–19. https://doi.org/10.1016/j.jiec.2018.05.020.

Gbadamosi, A.O., Junin, R., Manan, M.A., Agi, A., Yusuff, A.S., 2019. An overview of chemical enhanced oil recovery, recent advances and prospects. Int. Nano Lett. 9, 171–202. https://doi.org/10.1007/s40089-019-0272-8.

Guang, Z.H., Caili, D.A., Qing, Y.O., 2018. Characteristics and displacement mechanisms of the dispersed particle gel soft heterogeneous compound flooding system. Petrol. Explor. Dev. 45, 481–490. https://doi.org/10.1016/S1876-3804(18)30053-3.

He, L., Lin, F., Li, X., Sui, H., Xu, Z., 2015. Interfacial sciences in unconventional petroleum production: from fundamentals to applications. Chem. Soc. Rev. 44, 5446–5494. https://doi.org/10.1039/C5CS00102A.

Hou, J., Lin, S., Zhang, M., 2022. Ionic-liquid-enhanced solvent extraction mechanism: a novel concept. J. Environ. Chem. Eng., 107899 https://doi.org/10.1016/j.jece.2022.107899.

Jiang, H.J., Atkin, R., Warr, G.G., 2018. Nanostructured ionic liquids and their solutions: recent advances and emerging challenges. Curr. Opin. Green Sustain. Chem. 12, 27–32. https://doi.org/10.1016/j.cogsc.2018.05.003.

Joonaki, E., Gahrooei, H.R.E., Ghanaatian, S., 2016. Experimental study on adsorption and wettability alteration aspects of a new chemical using for enhanced oil recovery in carbonate oil reservoirs. J. Unconv. Oil Gas Resour. 15, 11–21. https://doi.org/10.1016/j.juogr.2016.05.001.

Kapitanov, I.V., Jordan, A., Karpichev, Y., Spulak, M., Perez, L., Kellett, A., Kümmerer, K., Gathergood, N., 2019. Synthesis, self-assembly, bacterial and fungal toxicity, and preliminary biodegradation studies of a series of L-phenylalanine-derived surface-active ionic liquids. Green Chem. 21, 1777–1794. https://doi.org/10.1039/C9GC00030E.

Kharazi, M., Saien, J., 2022a. Mechanism responsible altering in interfacial tension and emulsification of the crude oil-water system with nano Gemini surface active ionic liquids, salts and pH. J. Pet. Sci. Eng. 219, 111090. https://doi.org/10.1016/j.petrol.2022.111090.

Kharazi, M., Saien, J., 2022b. Upgrading the properties of the crude oil–water system for eor with simultaneous effects of a homologous series of nanogemini surface-active ionic liquids, electrolytes, and pH. ACS Omega 7, 40042–40053. https://doi.org/10.1021/acsomega.2c04741.

Kharazi, M., Saien, J., Asadabadi, S., 2022. Review on amphiphilic ionic liquids as new surfactants: from fundamentals to applications. Top. Curr. Chem. 380, 1–44. https://doi.org/10.1007/s41061-021-00362-6.

Kharazi, M., Saien, J., Torabi, M., Zolfigol, M.A., 2023. Green nano multicationic ionic liquid based surfactants for enhanced oil recovery: a comparative study on design and applications. J. Mol. Liq., 122090 https://doi.org/10.1016/j.molliq.2023.122090.

Kharazi, M., Saien, J., Yarie, M., Zolfigol, M.A., 2019. Different spacer homologs of gemini imidazolium ionic liquid surfactants at the interface of crude oil-water. J. Mol. Liq. 296, 111748. https://doi.org/10.1016/j.molliq.2019.111748.

Kharazi, M., Saien, J., Yarie, M., Zolfigol, M.A., 2020. The superior effects of a long chain gemini ionic liquid on the interfacial tension, emulsification and oil displacement of crude oil-water. J. Pet. Sci. Eng. 195, 107543. https://doi.org/10.1016/j.petrol.2020.107543.

Kharazi, M., Saien, J., Yarie, M., Zolfigol, M.A., 2021. Promoting activity of gemini ionic liquids surfactant at the interface of crude oil-water. Pet. Res. 117, 113–123. https://doi.org/10.22078/PR.2020.4130.2874.

Kumar, N., Mandal, A., 2018. Thermodynamic and physicochemical properties evaluation for formation and characterization of oil-in-water nanoemulsion. J. Mol. Liq. 266, 147–159. https://doi.org/10.1016/j.molliq.2018.06.069.

Lan, M., Wang, X., Chen, P., Zhao, X., 2016. Effects of surface tension and wood surface roughness on impact splash of a pure and multi-component water drop. Case Stud. Therm. Eng. 8, 218–225. https://doi.org/10.1016/j.csite.2016.07.006.

Liu, G., Gu, D., Liu, H., Ding, W., Luan, H., Lou, Y., 2012. Thermodynamic properties of micellization of Sulfobetaine-type Zwitterionic Gemini Surfactants in aqueous solutions–A free energy perturbation study. J. Colloid Interface Sci. 375, 148–153. https://doi.org/10.1016/j.jcis.2012.02.027.

Liu, C., Si, X., Yan, S., Zhao, X., Qian, X., Ying, W., Zhao, L., 2021. Development of the C_{12}Im-Cl-assisted method for rapid sample preparation in proteomic application. Anal. Methods 13, 776–781. https://doi.org/10.1039/D0AY02079F.

Łuczak, J., Paszkiewicz, M., Krukowska, A., Malankowska, A., Zaleska-Medynska, A., 2016. Ionic liquids for nano- and microstructures preparation. Part 2: application in synthesis. Adv. Colloid Interface Sci. 227, 1–52. https://doi.org/10.1016/j.cis.2015.08.010.

Matsubara, H., Onohara, A., Imai, Y., Shimamoto, K., Takiue, T., Aratono, M., 2010.

Effect of temperature and counterion on adsorption of imidazolium ionic liquids at air–water interface. Colloids Surf. A Physicochem. Eng. Asp. 370, 113–119. https://doi.org/10.1016/j.colsurfa.2010.08.057.
Möbius, D., Miller, R., Fainerman, V.B., 2001. Surfactants: Chemistry, Interfacial Properties, Applications. Elsevier.
Motomura, K., Iwanaga, S.I., Yamanaka, M., Aratono, M., Matuura, R., 1982. Thermodynamic studies on adsorption at interaces: V. Adsorption from micellar solution. J. Colloid Interface Sci. 86, 151–157. https://doi.org/10.1016/0021-9797(82)90050-9.
Nacham, O., Martín-Pérez, A., Steyer, D.J., Trujillo-Rodríguez, M.J., Anderson, J.L., Pino, V., Afonso, A.M., 2015. Interfacial and aggregation behavior of dicationic and tricationic ionic liquid-based surfactants in aqueous solution. Colloids Surf. A Physicochem. Eng. Asp. 469, 224–234. https://doi.org/10.1016/j.colsurfa.2015.01.026.
Painter, P., Williams, P., Lupinsky, A., 2010. Recovery of bitumen from Utah tar sands using ionic liquids. Energy Fuel. 24, 5081–5088. https://doi.org/10.1021/ef100765u.
Pal, N., Kumar, N., Mandal, A., 2019. Stabilization of dispersed oil droplets in nanoemulsions by synergistic effects of the gemini surfactant, PHPA polymer, and silica nanoparticle. Langmuir 35, 2655–2667. https://doi.org/10.1021/acs.langmuir.8b03364.
Panchal, B., Chang, T., Qin, S., Sun, Y., Wang, J., Bian, K., 2020. Optimization of soybean oil transesterification using an ionic liquid and methanol for biodiesel synthesis. Energy Rep. 6, 20–27. https://doi.org/10.1016/j.egyr.2019.11.028.
Pavia, D.L., Lampman, G.M., Kriz, G.S., Vyvyan, J.A., 2014. Introduction to Spectroscopy. Cengage Learning.
Pillai, P., Mandal, A., 2019. Wettability modification and adsorption characteristics of imidazole-based ionic liquid on carbonate rock: implications for enhanced oil recovery. Energy Fuel. 33, 727–738. https://doi.org/10.1021/acs.energyfuels.8b03376.
Pillai, P., Mandal, A., 2022. Synthesis and characterization of surface-active ionic liquids for their potential application in enhanced oil recovery. J. Mol. Liq. 345, 117900. https://doi.org/10.1016/j.molliq.2021.117900.
Razzaghi-Koolaee, F., Mehrabianfar, P., Soulgani, B.S., Esfandiarian, A., 2022. A comprehensive study on the application of a natural plant-based surfactant as a chemical enhanced oil recovery (CEOR) agent in the presence of different ions in carbonate reservoirs. J. Environ. Chem. Eng., 108572 https://doi.org/10.1016/j.jece.2022.108572.
Rosen, M.J., Wang, H., Shen, P., Zhu, Y., 2005. Ultralow interfacial tension for enhanced oil recovery at very low surfactant concentrations. Langmuir 21, 3749–3756. https://doi.org/10.1021/la0400959.
Saien, J., Kharazi, M., Asadabadi, S., 2015. Adsorption behavior of short alkyl chain imidazolium ionic liquidsat *n*-butyl acetate+water interface: experiments and modeling. Iran. J. Chem. Eng. 12, 59–74.
Saien, J., Kharazi, M., Pino, V., Pacheco-Fernández, I., 2022. Trends offered by ionic liquid-based surfactants: applications in stabilization, separation processes, and within the petroleum industry. Separ. Purif. Rev. 164–192. https://doi.org/10.1080/15422119.2022.2052094.
Saien, J., Kharazi, M., Shokri, B., Torabi, M., Zolfigol, M.A., 2023. A comparative study on the design and application of new nano benzimidazolium gemini ionic liquids for curing interfacial properties of the crude oil–water system. RSC Adv. 13, 15747–15761. https://doi.org/10.1039/D3RA01783D.
Saien, J., Kharazi, M., Yarie, M., Zolfigol, M.A., 2019. Systematic investigation of a surfactant type nano gemini ionic liquid and simultaneous abnormal salt effects on crude oil/water interfacial tension. Ind. Eng. Chem. Res. 58, 3583–3594. https://doi.org/10.1021/acs.iecr.8b05553.
Sharma, P.S., Payagala, T., Wanigasekara, E., Wijeratne, A.B., Huang, J., Armstrong, D.W., 2008. Trigonal tricationic ionic liquids: molecular engineering of trications to control physicochemical properties. Chem. Mater. 20, 4182–4184. https://doi.org/10.1021/cm800830v.
Stauffer, C.E., 1965. The measurement of surface tension by the pendant drop technique. J. Phys. Chem. 69, 1933–1938. https://doi.org/10.1021/j100890a024.
Steudte, S., Bemowsky, S., Mahrova, M., Bottin-Weber, U., Tojo-Suarez, E., Stepnowski, P., Stolte, S., 2014. Toxicity and biodegradability of dicationic ionic liquids. RSC Adv. 4, 5198–5205. https://doi.org/10.1039/C3RA45675G.
Stubenrauch, C., Fainerman, V.B., Aksenenko, E.V., Miller, R., 2005. Adsorption behavior and dilational rheology of the cationic alkyl trimethylammonium bromides at the water/air interface. J. Phys. Chem. B 109, 1505–1509. https://doi.org/10.1021/jp046525l.
Tamayo-Mas, E., Mustapha, H., Dimitrakopoulos, R., 2016. Testing geological heterogeneity representations for enhanced oil recovery techniques. J. Pet. Sci. Eng. 146, 222–240. https://doi.org/10.1016/j.petrol.2016.04.027.
Yazhou, Z., Demin, W., Zhipeng, W., Rui, C., 2017. The formation and viscoelasticity of pore-throat scale emulsion in porous media. Petrol. Explor. Dev. 44, 111–118. https://doi.org/10.1016/S1876-3804(17)30014-9.
Zhang, L., Geng, Y., Duan, W., Wang, D., Fu, M., Wang, X., 2009. Ionic liquid-based ultrasound-assisted extraction of fangchinoline and tetrandrine from Stephaniae tetrandrae. J. Separ. Sci. 32, 3550–3554. https://doi.org/10.1002/jssc.200900413.
Zhang, W., Huang, G., Wei, J., Li, H., Zheng, R., Zhou, Y., 2012. Removal of phenol from synthetic waste water using Gemini micellar-enhanced ultrafiltration (GMEUF). J. Hazard Mater. 235–236, 128–137. https://doi.org/10.1016/j.jhazmat.2012.07.031.
Zhou, H., Zhu, Y., Peng, T., Song, Y., An, J., Leng, X., Yi, Z., Sun, Y., Jia, H., 2016. Systematic study of the effects of novel halogen-free anionic surface active ionic liquid on interfacial tension of water/model oil system. J. Mol. Liq. 223, 516–520. https://doi.org/10.1016/j.molliq.2016.08.080.